ISSN 1392–1320 MATERIALS SCIENCE (MEDŽIAGOTYRA). Vol. 25, No. 2. 2019

Mössbauer Spectroscopy and Magnetic Properties of $Bi_{0.8}Ca_{0.2-x}Sr_xFeO_3$ Nanoparticles by Sol-gel Method

Jin Pei LIN [1, 2], Ze Ping GUO [1], Qing LIN [1, 2]*, Yun Long WANG [1], Kang Ling HUANG [1], Yun HE [1, 3]

[1] *College of Physics and Technology, Guangxi Normal University, Guilin 541004, P.R.China*
[2] *Guangxi Key Laboratory of Nuclear Physics and Nuclear Technology, Guangxi Normal University, Guilin 541004, P.R.China*
[3] *Sate Key Laboratory for Chemistry and Molecular Engineering of Medicinal Resources, Guangxi Normal University, Guilin 541004, P.R.China*

crossref http://dx.doi.org/10.5755/j01.ms.25.2.19456

Received 10 November 2017; accepted 18 February 2018

Doping at A/B-sites can effectively improve the physical properties of perovskite ferrites. In this study, the performance of $Bi_{0.8}Ca_{0.2-x}Sr_xFeO_3$ was investigated using the sol-gel autocombustion method. The results show that with an increase in x value, the grain size first increases and then decreases. With an increase in the doping concentration, the reunion phenomenon reduces, but the smoothness and flatness of the samples are also destroyed. Moreover, with increasing Sr^{2+} concentration, particle growth is inhibited, resulting in smaller particle sizes. When the Sr^{2+} concentration increases to a certain value, the environment becomes advantageous for particle growth and therefore the particle size increases. For x = 0.13, small particles are obtained. With increasing Sr^{2+} concentration, the spatial modulation of the spin structure is destroyed, the lattice distorts, and the magnetic force is freed. Mössbauer spectrum measurements shows that when the Ca^{2+} concentration is greater than the Sr^{2+} concentration, Sr^{2+} ions replace Ca^{2+} ions; as a result, A-A magnetic superexchange diminishes, leading to a decrease in the hyperfine field. Appropriate doping of $BiFeO_3$ can improve its coercivity and refine its grains and result in a larger magnetic force.
Keywords: Sr-substituted, perovskite, structure, magnetic properties, Mössbauer.

1. INTRODUCTION

A multiferroic material can simultaneously show two or more basic magnetic properties including ferromagnetism, antiferromagnetism, and ferroelectricity. One such novel material is elastic iron [1 – 3]. Multiferroic materials have attracted much research attention owing to their interesting properties. At present, they are widely used in the field of information storage, microwave, sensors, and converters [4 – 5]. $BiFeO_3$ is a multiferroic material with a rhombohedral distorted perovskite structure. It is a rare material that simultaneously shows weak ferroelectricity ($T_C \approx 830$ °C) and ferromagnetism ($T_N \approx 370$ °C) [6 – 8]; therefore, it has been studied extensively. However, it is difficult to prepare pure-phase $BiFeO_3$ because Bi can volatilize relatively easily during synthesis and the Fe valence fluctuates. At present, $BiFeO_3$ is mainly synthesized by the hydrothermal method [9], sol-gel [10], and coprecipitation method [11]. As Bi in $BiFeO_3$ can volatilize easily, a second phase such as $Bi_{25}FeO_{40}$ or $Bi_2Fe_4O_9$ is formed. In addition, the large leakage current of $BiFeO_3$ makes it difficult to achieve good magnetoelectric properties. Doping can reduce the volatility of Bi and greatly improve the magnetoelectric properties of $BiFeO_3$ [12]. Many studies have reported the doping of $BiFeO_3$ at the A site by alkaline earths such as Ca, Mg, Sr, and Ba [13 ,14, 15]. However, few studies have reported on double-doping at the A site by alkaline earths, such as doping using Ca and Mg, Ca and Sr, or Ba and Ca.

In this study, we aimed to investigate the performance of $Bi_{0.8}Ca_{0.2-x}Sr_xFeO_3$ (x = 0.04 ~ 0.20) by using the sol-gel autocombustion method. This study had three main objectives: (1) to use the sol-gel autocombustion method to investigate the influence of the double-doping content of alkaline earth ions on the structure by synthetizing a sample with a single-phase spinel structure; (2) to investigate the influence of the doping content by synthesizing homogeneously distributed and well-crystallized ferrite nanopowder samples; and (3) to investigate the magnetic properties of samples with different double-doping contents of alkaline earth ions at the A site by Mössbauer spectroscopy and to confirm the magnetic behavior of $Bi_{0.8}Ca_{0.2-x}Sr_xFeO_3$ nanoferrites.

2. EXPERIMENTAL SECTION

2.1. Sample synthesis

Fig. 1 shows the synthesis route of $Bi_{0.8}Ca_{0.2-x}Sr_xFeO_3$ powder prepared using the polyacrylamide sol-gel method. Identical mol amounts of $Bi(NO_3)_3{\cdot}5H_2O$ and $Fe(NO_3)_3{\cdot}9H_2O$ are added to dilute nitric acid (1.6 mol/L). Then, some ethylenediamine tetraacetic acid is added as a complexing agent. Appropriate amounts of glucose (20 g/100 ml), $Ca(NO_3)_2{\cdot}6H_2O$, and $Sr(NO_3)_2$ are added according to the proportion, and the mixture is stirred constantly. Then, acrylamide monomer with metal cations is added in the molar ratio of 1:9, and the precursor

* Corresponding author. Tel.: +86-773-5840785; fax: +86-773-5811173.
E-mail address: *hy@gxnu.edu.cn* (Q. Lin)

reaction liquids are mixed completely. The precursor solution is heated at 70 ℃ in a water bath for 5 – 10 min to obtain a transparent solution. Then, an appropriate amount of ammonia is added to the transparent solution to adjust its pH value to ≈ 3. Finally, the solution is heated at 80 ℃ for 5 – 7 h in the water bath until a dry wet gel is obtained. The wet gel is placed in a drying chamber and dried at 120 ℃ for 5 h to obtain a dry gel. Then, the dry gel is combusted in air by adding drops of anhydrous ethanol propellant to obtain a fluffy powder. This powder is ground and placed in a muffle furnace, in which it is calcined at 600 ℃ for 3 h to obtain a fluffy yellow mud powder.

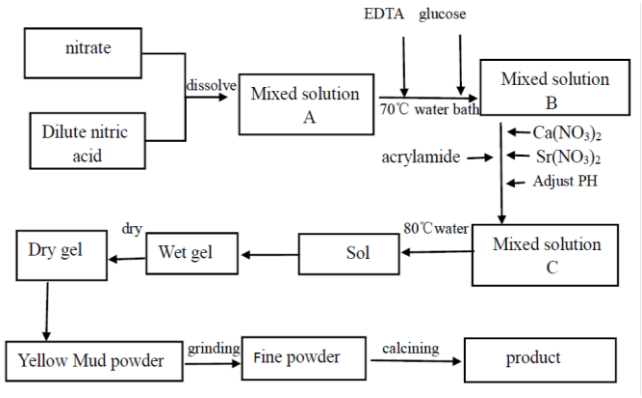

Fig. 1. Synthesis route of $Bi_{0.8}Ca_{0.2-x}Sr_xFeO_3$ powder by polyacrylamide sol-gel method

2.2. Sample characterization

The crystalline structure was investigated by x-ray diffraction (XRD, Rigaku D/max- 2500V/PC) with Cu Kα radiation (λ = 0.15405 nm). The micrographs were obtained by scanning electron microscopy (SEM, NoVa™ Nano SEM 430). The Mössbauer spectrum was performed at room temperature, using a conventional Mössbauer spectrometer (MS, Fast Com Tec PC-moss II), in constant acceleration mode. The γ-rays were provided by a ^{57}Co source in a rhodium matrix. Magnetization measurements were carried out with superconducting quantum interference device (MPMS-XL-7, Quantum Design) at room temperature.

3. RESULTS AND DISCUSSION

3.1. Structure analysis of $Bi_{0.8}Ca_{0.2-x}Sr_xFeO_3$

Many studies have reported on the doping of $BiFeO_3$ at the A site by alkaline earths such as Ca, Mg, Sr, and Ba. For example, Khomchenko *et al.* [15] investigated the influence of different Ca^{2+} and Sr^{2+} doping ratios on the structure analysis of $Bi_{0.7}A_{0.3}FeO_3$ (A = Ca^{2+}, Sr^{2+}) samples. However, few studies have reported on double-doping at the A Site by alkaline earths, such as doping using Ca and Sr. Fig. 2 shows the room-temperature X-ray diffraction pattern of $Bi_{0.8}Ca_{0.2-x}Sr_xFeO_3$ (x=0.04~0.20) calcined at 600 ℃ for 3 h. All diffraction peaks appear to be attributable to a pure phase, and all of them conform to the standard diffraction peaks (JCPDS card no. 861518) of $BiFeO_3$ with perovskite structure. The impurity in these samples is undetectable, and it shows no significant change when the doping content is increased from 0.04 to 0.20, as shown in Fig. 2 a; this result agrees well with that of Chauhan's study [2].

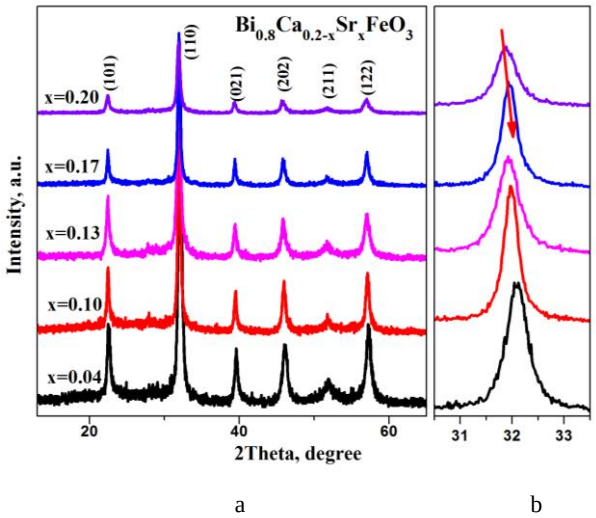

Fig. 2. XRD patterns of various contents for $Bi_{0.8}Ca_{0.2-x}Sr_xFeO_3$ samples calcined at 600 ℃ for 3 h

The diffraction peak changes with Ca^{2+} and Sr^{2+} codoping; however, no clear impurity phase with good crystallinity can be seen. The diffraction peak trends toward low 2θ angles, as shown in Fig. 2 a. This may be due to the replacement radius of Sr^{2+} (R_{Sr} = 0.118 nm) being greater than that of Ca^{2+} (R_{Ca} = 0.1 nm) owing to the distortion of the crystal structure [13, 14]. Ca^{2+} and Sr^{2+} ions can enter the $BiFeO_3$ perovskite crystal structure and form a solid solution; this is consistent with the conclusion of Khomchenko *et al.* [15]. Furthermore, with an increase in x value, the diffraction peak intensity of the samples gradually decreases, because codoping by alkaline earth ions reduces the crystalline effect. It should be noted that the half high width of the diffraction peak first increases and then decreases with an increase in x value. When only Sr is doped (x = 0.2), the half high width of the diffraction peak tends to increase again [16].

Fig. 2 b shows an enlarged view of the (110) peaks of $Bi_{0.8}Ca_{0.2-x}Sr_xFeO_3$ nanoferrites. This figure shows that all diffraction peaks widen and move in the direction of increasing diffraction angle with increasing amounts of Ca. Fig. 2 b also shows the lattice parameters for $Bi_{0.8}Ca_{0.2-x}Sr_xFeO_3$ (x = 0.04 ~ 0.20). With increasing proportion of doped Sr, the diffraction peaks markedly move in the increasing 2θ direction; this agrees well with Khomchenko's results [17].

The Scherrer formula is given as follows [18, 19]:

$$D = K\lambda/\beta\cos\theta, \quad (1)$$

where K is the Scherrer constant; β is the half high width of the peak; D is the grain size; λ is the X-ray wavelength; and θ is the diffraction angle. The wider the peak, the smaller the grains can be, and the narrower the peak, the bulkier the grains can be. Therefore, the grain size first increases and then decreases with an increase in x value. As mentioned above, when only Sr is doped (x = 0.2), it tends to increase, as shown in Fig. 3.

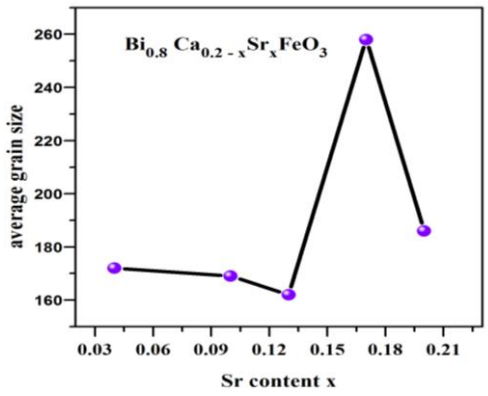

Fig. 3. Change in average grain size with proportion of doped Sr value

3.2. SEM microstructure studies of $Bi_{0.8}Ca_{0.2-x}Sr_xFeO_3$

Fig. 4 shows scanning electron microscope (SEM) images of $Bi_{0.8}Ca_{0.2-x}Sr_xFeO_3$ calcined at 600 ℃ for 3 h. The particle size of the samples decreases and then increases with an increase in the doping amount, and the reunion phenomenon reduces. This suggests that an increase in the Sr^{2+} concentration inhibits particle growth, resulting in smaller particle size in the samples. When the Sr^{2+} concentration increases to a certain value, the environment becomes advantageous for particle growth and therefore the particle size increases. Therefore, the grain size can be refined effectively by controlling the Sr^{2+} concentration in the samples [20, 21].

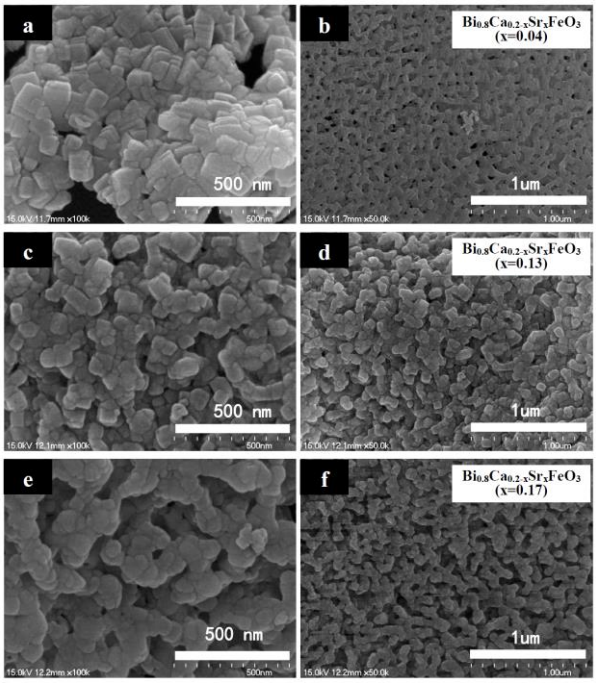

Fig. 4. SEM micrographs of $Bi_{0.8}Ca_{0.2-x}Sr_xFeO_3$ calcined at 600 ℃ for 3 h

A particle size distribution analysis software is used to obtain a histogram of the sample's particle size distribution, as shown in Fig. 5. For x = 0.04, the particle size is mainly concentrated in the range of 71 – 89 nm. Then, for x = 0.13, the particle size obviously decreases to the range of 60 – 71 nm. However, for x = 0.17, the particle size increases and is mainly concentrated in the range of 69 – 87 nm. These results indicate that with an increase in Sr^{2+} concentration, the particle size first decreases and then increases; these results are consistent with the XRD results [22, 23].

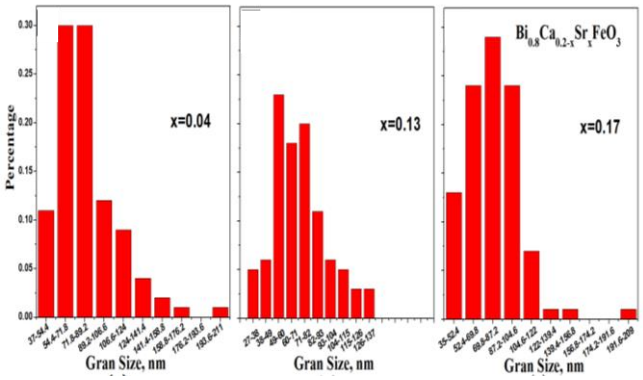

a b c

Fig. 5. Histogram of $Bi_{0.8}Ca_{0.2-x}Sr_xFeO_3$ (x=0.04, 0.13, 0.17) samples' particle size distribution

3.3. Magnetic studies of $Bi_{0.8}Ca_{0.2-x}Sr_xFeO_3$

Fig. 6 shows the magnetic hysteresis curves of $Bi_{0.8}Ca_{0.2-x}Sr_xFeO_3$ (x = 0.04, 0.13, 0.17) calcined at 600 ℃ for 3 h. All samples almost reach saturation magnetization when the field is 10000 Oe. Table 1 shows the corresponding parameters.

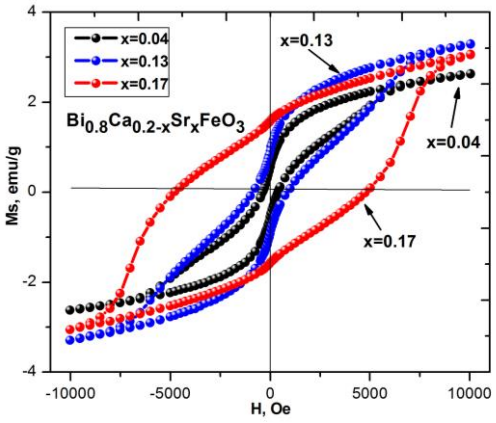

Fig. 6. Hysteresis curves of $Bi_{0.8}Ca_{0.2-x}Sr_xFeO_3$ calcined at 600 ℃ for 3 h with different Ca^{2+} and Sr^{2+} doping contents (x = 0.04, 0.13, 0.17)

Table 1 shows that with Sr^{2+} doping, the saturation magnetization of the samples first increases and then decreases. The saturation magnetization can be expressed as follows [16, 17, 24]:

$$\sigma_s = \frac{5585 \times n_B}{M} \quad (2)$$

where n_B is the magnetic moment (unit: Bohr magneton) and M, the relative molecular mass. The relative molecular mass of the sample increases with increasing Sr^{2+} doping. Fig. 6 and Table 1 show that with an increase in x value, the remanent magnetization and coercive force of the samples increase substantially.

Table 1. Saturation magnetization (*M*s), coercivity (*H*c), residual magnetization (*M*r), and magnetic moment (n_B) of $Bi_{0.8}Ca_{0.2-x}Sr_xFeO_3$ calcined at 600 ℃ for 3 h

Content, *x*	*M*s, emu/g	*H*c, Oe	*M*r, emu/g	n_B
0.04	2.6222	376.1749	0.5618	0.1319
0.13	3.2832	877.8747	0.9169	0.1659
0.17	3.0547	4764.8620	1.5820	0.1534

Table 2. Mössbauer parameters including isomer shift (I.S.), quadrupole splitting (Q.S.), magnetic hyperfine field (H_{hf}), line width (Γ), and absorption area (A_0) of $Bi_{0.8}Ca_{0.2-x}Sr_xFeO_3$ (*x* = 0.04, 0.13, 0.17) annealed at 600 ℃ for 3 h

Content, *x*	I.S., mm/s	Q.S., mm/s	H_{hf}, T	*Γ*, mm/s	A_0, %
0.04	0.3847	-0.0556	48.9627	0.5969	10.5160
0.13	0.2591	0.0070	48.7614	0.5974	9.4367
0.17	0.2419	-0.0325	48.8988	0.5604	18.672

In particular, when *x* value increases from 0.13 to 0.17, the remanent magnetization increases from 0.9169 to 1.5820 emu/g, respectively, and the coercive force increases more than five-fold from 877.8747 to 4764.8620 Oe, respectively. These large changes are attributable to the increase in Sr^{2+} content in the sample; this increase distorts the lattice, destroys the spatial modulation of the spin structure, and frees the magnetic force, resulting in a larger magnetic force [19, 25, 26].

3.4. Mössbauer spectroscopy study of $Bi_{0.8}Ca_{0.2-x}Sr_xFeO_3$

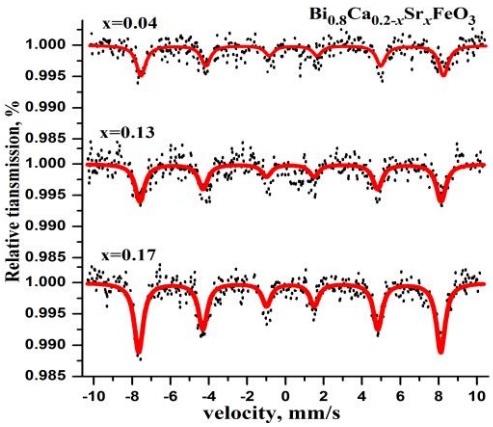

Fig. 7. Mössbauer spectra of $Bi_{0.8}Ca_{0.2-x}Sr_xFeO_3$ (*x* = 0.04, 0.13, 0.17) calcined at 600 ℃ for 3 h

Fig. 7 shows the Mössbauer spectra of $Bi_{0.8}Ca_{0.2-x}Sr_xFeO_3$ (*x* = 0.04, 0.13, 0.17). The spectral data of all samples are analyzed used Mösswinn 3.0 software, and all spectral peaks are fitted with a set of six lines. All maps show a six-line spectrum, indicating that the samples are ferromagnetic. With an increase in Sr^{2+} concentration, an increasing number of black spots concentrate around the red spectrum line and the sinking peak becomes much larger.

Table 2 shows the isomeric shift (I.S.), quadrupole splitting (Q.S.), hyperfine field (H_{hf}), line width (Γ), and relative parameters such as absorption area (A_0) of samples that are calcined at 600 ℃ for 3 h and then naturally cooled to room temperature. From Fig. 7 and Table 2, the Mössbauer spectrum line width parameter values (Γ), relative absorption area, lattice distribution, Bi ions, Sr^{2+} ions, and Fe^{3+} ions can be determined. With an increase in Sr^{2+} concentration, the I.S. decreases. With a change in the concentration of Ca^{2+} and Sr^{2+} ions, the distance between Fe^{3+} ions and O ions in the lattice changes. This, in turn, affects the s orbital's electron cloud overlap [18, 27, 28] and eventually leads to a change in IS. Based on literature [19], I.S. for Fe^{2+} ions lies in the range 0.6 – 1.7 mm/s, and that for Fe^{3+} ions lies in the range of 0.1 – 0.5 mm/s. The I.S. values in Table 2 indicate that iron is in the Fe^{3+} state. The H_{hf} first increases and then decreases with an increase in the Sr^{2+} concentration. This is because when the Ca^{2+} concentration is greater than the Sr^{2+} concentration, Sr^{2+} ions replace Ca^{2+} ions; as a result, A-A magnetic superexchange diminishes , leading to a decrease in H_{hf} [29, 30]. When the Ca^{2+} concentration is smaller than the Sr^{2+} concentration, the opposite results are obtained. All Q.S. values of samples that show six-line magnetic peaks are very small and can be ignored. This suggests that the concentration of Ca^{2+} and Sr^{2+} ions in the $Bi_{0.8}Ca_{0.2-x}Sr_xFeO_3$ sample has little impact on Q.S. [31]. Furthermore, the charge distribution around the nucleus of perovskite ferrite is symmetric, which could be caused by a variation in the ratio of the Fe^{2+}/Fe^{3+} valence states [32, 33, 34].

4. CONCLUSIONS

In this study, the polyacrylamide sol-gel method was used to synthesize $Bi_{0.8}Ca_{0.2-x}Sr_xFeO_3$ nanoferrites. With an increase in *x* value, no impurity was seen in the sample. With an increase in the Sr^{2+} concentration, as the replacement radius of Sr^{2+} ions (R_{Sr} = 0.118 nm) is greater than that of Ca^{2+} ions (R_{Ca} = 0.1 nm), the crystal structure distorts and the diffraction peaks shift toward low angles. In addition, with an increase in Sr^{2+} concentration, the half high width of the diffraction peak first increases, then decreases, and finally increases again. These results show that changes in the Ca^{2+} and Sr^{2+} concentrations can directly affect grain growth. Doping can reduce the reunion phenomenon and also reduce the smoothness and flatness of the grain surface. Mössbauer spectrum measurements show that when the Ca^{2+} concentration is greater than the Sr^{2+} concentration, Sr^{2+} ions replace Ca^{2+} ions; as a result, A-A magnetic superexchange diminishes, leading to a decrease in H_{hf}. With an increase in Sr^{2+} concentration, the coercive force of the sample changes greatly. As the Ca^{2+}

and Sr^{2+} concentrations in the sample change, the highly helical structure is damaged and the magnetic force is freed; this can result in an increase in the magnetic force. Appropriate doping of $BiFeO_3$ can improve its Hc and refine its grains and result in a larger magnetic force.

Acknowledgments

This work was financially supported by the National Natural Science Foundation of China (NO.11364004,11647309,11547307,11164002) and Innovation Project of Guangxi Graduate Education under Grant (NO.YCSW2017097). J.P. Lin, Z.P. Guo and Q. Lin contributed equally to this work. Y. He, Q. Lin and K.L. Huang participated in experimental design. J.P. Lin, Z.P. Guo and Y.L. Wang collects data. Q. Lin and Y. He is co-corresponding authors contributed equally to this study. All authors discussed the results and commented on the manuscript. And the project was funded by State Key Laboratory for Chemistry and Molecular Engineering of Medicinal Resources.

REFERENCES

1. **Niu, F., Gao, T., Qin, L., Chen, Z., Huang, Q., Zhang, N., Wang, S., Sun, X., Huang, Y.** Polyvinyl Alcohol (Pva)-Assisted Synthesis of $BiFeO_3$ Nanoparticles for Photo Catalytic Applications *Journal of New Materials for Electrochemical Systems* 18 (2) 2015: pp. 69 – 73.
2. **Chauhan, S., Kumar, M., Chhoker, S., Katyal, S.C., Singh, M.** Substitution Driven Structural and Magnetic Transformation in Ca-Doped $BiFeO_3$ Nanoparticles *RSC Advances* 6 (49) 2016: pp. 43080 – 43090. https://doi.org/10.1039/C6RA02316A
3. **Tlemçani, T.S., Bahraoui, T.E., Taibi, M., Belayachi, A., Schmerber, G., Dinia, A., Abd-Lefdil, M.** Abd-Lefdil. Effect of Nd Substitution on Physical Properties of Multiferroic Compound $BiFeO_3$ *Journal of Sol-Gel Science and Technology* 73 (3) 2015: pp. 673 – 678. https://doi.org/10.1007/s10971-015-3654-z
4. **Layek, S., Verma, H.C., Garg, A.** Enhancement in Magnetic Properties of Ba-Doped $BiFeO_3$ Ceramics by Mechanical Activation *Journal of Alloys Compounds* 651 2015: pp. 294 – 301. https://doi.org/10.1016/j.jallcom.2015.08.057
5. **Lazenka, V.V., Zhang, G., Vanacken, J., Makoed, I.I., Ravinski, A.F., Moshchalkov, V.V.** Corrigendum: Structural Transformation and Magnetoelectric Behaviour in $Bi_{1-x}Gd_xFeO_3$ Multiferroics *Journal of Physics D Applied Physics* 45 2012: pp. 125002. https://doi.org/10.1088/0022-3727/45/12/125002
6. **Tabares Muñoz, C., Rivera, J.P., Bezinges, A., Monnier, A., Schmid, H.** Measurement of the Quadratic Magnetoelectric Effect on Single Crystalline $BiFeO_3$ *Japanese Journal of Applied Physics* 24 (S2) 1985: pp. 1051 – 1053. https://doi.org/10.7567/JJAPS.24S2.1051
7. **Fischer, P., Polomska, M., Sosnowska, I., Szymanski, M.** Temperature Dependence of the Crystal and Magnetic Structures of $BiFeO_3$ *Journal of Physics C Solid State Physics* 13 (10) 2000: pp. 1931 – 1940. https://doi.org/10.1088/0022-3719/13/10/012
8. **Schmid, H.** Multi-Ferroic Magnetoelectrics *Ferroelectrics* 162 (1) 1994: pp. 665 – 685. https://doi.org/10.1080/00150199408245120
9. **Chen, L., Ren, W., Zhu, W., Ye, Z.G., Shi, P., Chen, X., Wu, X., Yao, X.**Improved Dielectric and Ferroelectric Properties in Ti-Doped $BiFeO_3$-$PbTiO_3$ Thin Films Prepared by Pulsed Laser Deposition *Thin Solid Films* 518 (6) 2010: pp. 1637 – 1640. https://doi.org/10.1016/j.tsf.2009.11.072
10. **Brinkman, K., Iijima, T., Nishida, K., Katoda, T., Funakubo, H.** The Influence of Acceptor Doping on the Structure and Electrical Properties of Sol-Gel Derived $BiFeO_3$ Thin Films *Ferroelectrics* 357 (1) 2007: pp. 35 – 40. https://doi.org/10.1080/00150190701527597
11. **Yotburut, B., Yamwong, T., Thongbai, P., Maensiri, S.** Synthesis and Characterization of Coprecipitation-Prepared La-Doped $BiFeO_3$ Nanopowders and Their Bulk Dielectric Properties *Japanese Journal of Applied Physics* 53 (53) 2014: pp. 1347 – 4065. https://doi.org/10.7567/JJAP.53.06JG13
12. **Gaur, A., Singh, P., Choudhary, N., Kumar, D., Shariq, M., Singh, K., Kaur, D.** Structural, Optical and Magnetic Properties of Nd-Doped $BiFeO_3$ Thin Films Prepared by Pulsed Laser Deposition *Physica B Condensed Matter* 406 (10) 2011: pp. 1877 – 1882. https://doi.org/10.1016/j.physb.2011.02.046
13. **Zhang, S.T., Zhang, Y., Lu, M.H., Du, C.L., Chen, Y.F., Liu, Z.G., Zhu, Y.Y., Ming, N.B.** Substitution-Induced Phase Transition and Enhanced Multiferroic Properties of $Bi_{1-x}La_xFeO_3$ Ceramics *Applied Physics Letters* 88 (16) 2006: pp. 162901. https://doi.org/10.1063/1.2195927
14. **Wu, M.S., Huang, Z.B., Han, C.X., Yuan, S.L., Lu, C.L., Xia, S. C.** Enhanced Multiferroic Properties of $BiFeO_3$ Ceramics by Ba and High-Valence Nb Co-Doping *Solid State Communications* 152 (24) 2012: pp. 2142 – 2146. https://doi.org/10.1016/j.ssc.2012.09.005
15. **Khomchenko, V.A., Kiselev, D.A., Vieira, J.M., Jian, L., Kholkin, A.L., Lopes, A.M.L., Pogorelov, Y.G., Araujo, J.P., Maglione., M.** Effect of Diamagnetic Ca, Sr, Pb, and Ba Substitution on the Crystal Structure and Multiferroic Properties of the $BiFeO_3$, Perovskite *Journal of Applied Physics* 103 (2) 2008: pp. 024105. https://doi.org/10.1063/1.2836802
16. **Yuan, G.L., Wing, Or.S., Chan, H.L.W.** Structural Transformation and Ferroelectric Paraelectric Phase Transition in $Bi_{1-x}La_xFeO_3$ (x=0-0.25) Multiferroic Ceramics *Journal of Physics D Applied Physics* 40 (40) 2007: pp. 1196 – 1200. https://doi.org/10.1088/0022-3727/40/4/043
17. **Khomchenko, V.A., Kiselev, D.A., Selezneva, E.K., Vieira, J.M., Lopes, A.M.L., Pogorelov, Y.G., Araujo, J.P., Kholkin, A.L.** Weak Ferromagnetism in Diamagnetically-Doped $Bi_{1-x}A_xFeO_3$, (A=Ca, Sr, Pb, Ba) Multiferroics *Materials Letters* 62 (12) 2008: pp. 1927 – 1929. https://doi.org/10.1016/j.matlet.2007.10.044
18. **Ahmed, M.A., El-Khawlani, A.A.** Enhancement of the Crystal Size and Magnetic Properties of Mg-Substituted Co Ferrite *Journal of Magnetism and Magnetic Materials* 9 (321) 2009: pp. 1959 – 1963. https://doi.org/10.1016/j.jmmm.2008.12.021
19. **Kumar, S., Farea, A.M.M., Batoo, K.M., Chan, G.L., Koo, B.H., Yousef, A. Alimuddin**.Mössbauer Studies of $Co_{0.5}Cd_xFe_{2.5-x}O_4$ ($0.0 \leqslant x \leqslant 0.5$) Ferrite *Physica B Condensed Matter* 403 (s19 – 20) 2008: pp. 3604 – 3607. https://doi.org/10.1016/j.physb.2008.06.001

20. **Widatallah, H.M., Al-Mamari, F.A.S., Al-Saqri, N.A.M., Gismelseed, A.M., Al-Omari, I.A., Al-Shahumi, T.M.H., Alhaj, A.F., Abo El Ata, A.M., Elzain, M.E.** Mössbauer and Magnetic Studies of $Mg_{1+2x}Sb_xFe_{2-3x}O_4$ Spinel Ferrites *Materials Chemistry and Physics* 140 (1) 2013: pp. 97 – 103. https://doi.org/10.1016/j.matchemphys.2013.03.005
21. **Hashim, M., Meena, S.S., Kotnala, R.K., Shirsath, S.E., Bhatt, P., Kumar, S., Şentürk, E., Kumar, R., Gupta, N., Alimuddin.** Exploring the Structural, Mössbauer and Dielectric Properties of Co^{2+}, Incorporated $Mg_{0.5}Zn_{0.5-x}Co_x Fe_2O_4$, Nanocrystalline Ferrite *Journal of Magnetism Magnetic Materials* 360 2014: pp. 21 – 33. https://doi.org/10.1016/j.jmmm.2014.01.047
22. **Lin, Y.H., Jiang, Q., Wang, Y., Nan, C.W., Chen, L., Yu, J.** Enhancement of Ferromagnetic Properties in $BiFeO_3$ Polycrystalline Ceramic by La Doping *Applied Physics Letters* 90 (17) 2007: pp. 172507. https://doi.org/10.1063/1.2732182
23. **Zhang, S., Luo, W., Wang, D., Ma, Y.** Phase Evolution and Magnetic Property of $Bi_{1-x}Dy_xFeO_3$ Ceramics *Materials Letters* 63 (21) 2009: pp. 1820 – 1822. https://doi.org/10.1016/j.matlet.2009.05.056
24. **Yuan, G.L., Or, S.W., Chan, H.L.W., Liu, Z. G.** Reduced Ferroelectric Coercivity in Multiferroic $Bi_{0.825}Nd_{0.175}FeO_3$ Thin Film *Journal of Applied Physics* 101 (2) 2007: pp. 024106. https://doi.org/10.1063/1.2423228
25. **Gao, F., Cai, C., Wang, Y., Dong, S., Qiu, X.Y., Yuan, G.L., Liu, J.M.** Preparation of La-Doped $BiFeO_3$ Thin Films with Fe^{2+} Ions on Si Substrates *Journal of Applied Physics* 99 (9) 2006: pp. 094105. https://doi.org/10.1063/1.2195368
26. **Yuan, G.L., Or, S.W., Liu, J.M., Liu, Z. G.**Structural Transformation and Ferroelectromagnetic Behavior in Single-Phase $Bi_{1-x}Nd_xFeO_3$ Multiferroic Ceramics *Applied Physics Letters* 89 (5) 2006: pp. 052905. https://doi.org/10.1063/1.2266992
27. **Reddy, V.R., Kothari, D., Gupta, A., Gupta, S.M.** Study of Weak Ferromagnetism in Polycrystalline Multiferroic Eu Doped Bismuth Ferrite *Applied Physics Letters* 94 (8) 2009: pp. 082505. https://doi.org/10.1063/1.3089577
28. **Naganuma, H., Miura, J., Okamura, S.** Ferroelectric, Electrical and Magnetic Properties of Cr, Mn, Co, Ni, Cu Added Polycrystalline $BiFeO_3$ Films *Applied Physics Letters* 93 (5) 2008: pp. 0529011 – 2529013. https://doi.org/10.1063/1.2965799
29. **He, Y., Lei, C., Lin, Q., Dong, J., Yu, Y., Wang, L.** Mössbauer and Structural Properties of La-Substituted $Ni_{0.4}Cu_{0.2}Zn_{0.4}Fe_2O_4$ Nanocrystalline Ferrite *Science of Advanced Materials* 7 (9) 2015: pp. 1809 – 1815. https://doi.org/10.1166/sam.2015.2394
30. **Rusakov, V.S., Pokatilov, V.S., Sigov, A.S., Matsnev, M.E., Gubaidulina, T.V.** Temperature Investigations of the Spatial Spin-Modulated Structure of Multiferroic $BiFeO_3$ by Means of Mössbauer Spectroscopy *Bulletin of the Russian Academy of Sciences Physics* 79 (6) 2015: pp. 708 – 711. https://doi.org/10.3103/S1062873815060271
31. **Wang, K.F., Liu, J.M., Ren Z.F.** Multiferroicity, The Coupling Between Magnetic and Polarization *Advances in Physics* 58 (4) 2009: pp. 321 – 448. https://doi.org/10.1080/00018730902920554
32. **Lv, H., Zhang, H., Zhang, B., Ji, G., He, Y., Lin, Q.** Proposed Electron Transmission Mechanism Between Fe^{3+}/Co^{2+} and Fe^{3+}/Fe^{3+} in Spinel Structure and its Practical Evidence on Quaternary $Fe_{0.5}Ni_{0.5}Co_2S_4$ *Journal of Materials Chemistry C* 4 (23) 2016: pp. 5476 – 5482. https://doi.org/10.1039/C6TC01695B
33. **Takahashi, K., Tonouchi, M.** Influence of Manganese Doping in Multiferroic Bismuth Ferrite Thin Films *Journal of Magnetism and Magnetic Materials* 310 (2) 2007: pp. 1174 – 1176. https://doi.org/10.1016/j.jmmm.2006.10.280
34. **Phokha, S., Pinitsoontorn, S., Rujirawat, S., Maensiri, S**. Polymer Pyrolysis Synthesis and Magnetic Properties of $LaFeO_3$ Nanoparticles *Physica B* 476 2015: pp. 55 – 60. https://doi.org/10.1016/j.physb.2015.07.021